Biomineralized Ferroptosis-Inducing Nanovaccine Based on Combination of Photothermal Therapy and Checkpoint Blockade for Melanoma

Siyu Ma
Shanghai Jiao Tong University
Jie Yang
Shanghai Jiao Tong University
Tianxu Fang
Shanghai Jiao Tong University
Jun Zhang
Shanghai Jiao Tong University
Xiuhua Pan
Shanghai Jiao Tong University
Yawen Wei
Shanghai Jiao Tong University
Ning Yang
Shanghai Jiao Tong University
Zengyi Liu
Shanghai Jiao Tong University
Qi Shen (qshen@sjtu.edu.cn)
Shanghai Jiao Tong University

Research Article

Keywords: tumor nanovaccine, biomineralization, ferroptosis, cancer immunotherapy, photothermal therapy

Posted Date: March 24th, 2022

DOI: https://doi.org/10.21203/rs.3.rs-1463934/v1

Abstract

Background: Until now, treatment of refractory tumors and uncontrolled metastasis has not yet achieved satisfactory therapeutic results due to the immunosuppressive tumor microenvironment. The crucial point is inadequate in vivo immune response after tumor initial cure ablation. Here, we proposed the construction of a photothermal nanovaccine based on biomineralized ovalbumin induced ferroptosis after near-infrared triggering. Fe^{3+} were chelated inside exogenous antigen ovalbumin by biomineralization, and photosensitizer IR820 was loaded on the outer layer by electrostatic incorporation. Cytotoxic T lymphocyte-associated protein 4 (CTLA-4) checkpoint blockade was combined to offer incomparable opportunities for high-effcient synergistic therapy which consists of ferroptosis, photothermal therapy and cancer immunotherapy.

Results: After injection treatment, Fe^{3+} in the vaccine consumed glutathione (GSH) in cells, affected the expression of GPX4 and initiated Fenton reaction, resulting in ferroptosis, which promoted the immunogenic cell death (ICD). After ICD initiation, released tumor endogenous antigens aroused immune cells activation together with ovalbumin. T cells were successfully recruited and infiltrated into tumor, promising the primary tumor received direct therapy and was effectively suppressed. The photothermal effect was triggered by near-infrared irradiation. Photothermal effect of nanovaccine effectively amplified mild immune response by ferroptosis. With combining with CTLA-4 checkpoint blockade, the related cytokines and other immune indicators all showed increasing levels, which had a significant inhibition effect on distal simulated metastases growth.

Conclusion: Fe@OVA-IR820 nanovaccine successfully treated primary and metastatic melanoma with combination therapy. Therefore, we could propose Fe@OVA-IR820 nanovaccine combined checkpoint blockade as a potential therapeutic strategy for melanoma treatment in the future.

Background

In recent centuries, cancer caused by malignant tumors has become an intimidation to human lifespan[1]. Cancer has always been considered a highly adaptable ecosystem, for which monotherapy has limited heterogeneity and is difficult to cure absolutely[2, 3]. Mainstream cancer means including excision, chemotherapy and radiotherapy, which have a narrow therapeutic effect against tumor in later period as reported[4]. For example, surgery has been the primary treatment for most solid tumors[5]. However, after tumor tissue is removed, the residual tumor cells after treatment sometimes cunningly evade the immune response of the body[6] and result in uncontrollable tumor metastasis or recurrence[7], which can be prevented through immunotherapy[4] to some extent. Many researches have exhibited that activated immune system shows a significant effect in treating advanced or metastatic tumors during traditional monotherapy[8–11]. Combination therapy strategy based on multiple treatment methods is the main trend of future research[12–14] and multimodal therapies combining various treatment modalities are being extensively studied.

Cancer immunotherapy has attracted great attention recently for favorable prognosis through exploiting immune system to attack tumor cells autonomously. Related immunotherapies proposed include cytokine therapy, checkpoint blocking therapy, and cancer vaccines, etc[15–17]. Among these therapies, cancer vaccines have been shown to possess the ability to trigger long-lasting specific immune responses in particular, at the tumor site after injection[18, 19]. Compared to the vaccine which targets one or two antigens alone, the vaccine system composed of whole tumor lysates can stimulate the anti-tumor immune response more effectively and induce the immune response with higher performance[20]. Many efforts have been put into the development and research of nanovaccines[21, 22], and there is still a great need for manufacturing effective nanovaccines for tumor immunotherapy with minimal preparing methods[23], considering mass production could be achieved in a short time.

Ferroptosis was discovered and reported of late years, which is motivated by inactivation of glutathione peroxidase (GPX4), and hence upsetting intracellular reactive oxygen species (ROS) balance[24]. The homoeostatic process between the production and clearance of hydroxyl free radicals is broken[25] and its accumulation further leads to increases in ROS and lipid peroxidation products (LPO), which causing ferroptosis to kill tumor cells[26, 27]. Damage associated molecular patterns (DAMPs) as typical ICD bio-markers are increased with more secretion due to the ferroptosis procedure, which make ICD a promising treatment that can turn rupture cells after death into vaccine to overcome disease recurrence[28]. Ferroptosis can effectively inhibit tumor growth while producing associated immunogenicity[29]. Therefore, an immunological strategy to induce ICD by inducing cell ferroptosis is feasible. Moreover, photothermal therapy (PTT) is a therapy with proven efficacy for cancer tumor ablation. The immunogenicity produced by ferroptosis was proved to be mild[29] and the effect of PTT further strengthens the systemic anti-tumor immune responses operated by ferroptosis, including the expression and secretion of cytokines[30, 31].

Biomineralization is becoming research hotspot of nanomaterials synthesis lately, which using biological nanostructures as templates. With the reputation of time-honored model antigen, ovalbumin (OVA) is picked to construct vaccine. Related reports have suggested that proteins can serve as potential templates for biomineralized nanoparticles[32, 33].

In this work, we tried to construct a photothermal ferroptosis-inducing nanovaccine for melanoma therapy, aiming at acquiring adequate long-lasting tumor-specific immune responses to trigger effective cancer immunotherapy. The checkpoint blockade was combined to achieve satisfactory aftereffects. Considering the important role of iron element in ferroptosis, our design anchored Fe^{3+} ions to the OVA-composed vaccine center, coated with IR820 material with excellent photothermal properties. The combination of nanoparticles is novel. The released iron ions by nanovaccine in acidic environment could consume intracellular GSH and push the amplification of Fenton reaction, promoting accumulation of ROS and LPO and triggering ferroptosis. Tumor cells became immunogenic through stimulation by ferroptosis, and this mild immune response could be effectively amplified by PTT. The exogenous antigen OVA could more effectively induce a strong and sufficient autonomous immune response, together with released endogenous antigens to awaken downstream DC cells and induce high-quality immunity. This

strategy allows effective treatment of primary tumors that received direct treatment. The therapeutic effect was enhanced through combination of anti-CTLA-4 checkpoint blockade, these two components combined to form a therapeutic regiment that can efficaciously induce ablation of tumor in situ and at distant site.

Materials And Methods

Materials

Ferric chloride hexahydrate was bought from Aladdin Reagent Co., Ltd. (Shanghai, China). OVA (Biotech Grade) was got from Shanghai Macklin Biochemical Co., Ltd. (Shanghai, China). Ferrostatin − 1 (Fer-1), phthalaldehyde, new indolyanine green, deferroamine (DFO), glutathione (GSH), 30% hydrogen peroxide were bought from Bide Pharmatech Ltd. (Shanghai, China). Crystal violet came from Sangon Biotech (Shanghai) Co., Ltd. (Shanghai, China). Thiazole blue (MTT), 4', 6-diamidine-2-phenylindole (DAPI) were ordered from Shanghai Titan Scientific Co., Ltd. (Shanghai, China). All other chemicals were obtained from domestic reagent suppliers and could be used as an analytical grade.

Cells and Animals

B16-OVA cell lines were purchased from Institute of Biochemistry and Cell Biology (Shanghai, China). Cells were cultured in f\high- glucose DMEM medium in a humidified incubator at 37°C and 5% CO_2.

Healthy male C57BL/6 mice (6-8weeks) were bought from Shanghai Jihui Laboratory Animal Care Co.,Ltd. (Shanghai, China) and fed at the branch platform of School of Pharmacy, Laboratory Animal Center of University. The feeding conditions were 25 ± 2°C temperature and 50 ± 5% humidity.

Methods

Preparation methods and related characterization

2 mL ferric chloride solution (200 mM) was slowly dripped into 20 mL of freshly prepared OVA aqueous solution (0.025 g/ mL) under gentle stirring at room temperature. Amino acid residues in protein molecules captured and chelated metal ions. Then the pH was regulated to 12 through adding aqueous solution of NaOH (2 M). After the system pH changed, the captured ions undergo formed iron hydroxide in situ with rapid growth. Adjusted the pH value to 4 with 0.5% (W/V) citric acid after 2 hours, the denatured proteins were removed by centrifugation (10000 rpm, 10 min) to obtain Fe@OVA nanoparticles. Then 2 mL IR820 liquor (1 mg/mL) was instilled to the remaining mixture and guided IR820 to coat on the surface of Fe@OVA nanoparticles through electrostatic adsorption. After stirring for 24 hours, Fe@OVA-IR820 nanovaccine was formed. The removal of unloaded free IR820 was carried out by centrifugation and ultrafiltration (10 kDa)

The average diameters and ζ-potentials of Fe@OVA and Fe@OVA-IR820 were checked by dynamic light scattering (Zetasizer ZS90, Malvern, UK). Images of nanovaccine were obtained by 120kV transmission

electron microscope (TEM) (Talos L120C G2, Thermo Fisher Scientific, USA).

Release of iron ions was tested by a microplate reader (Varioskan Flash, Thermo Fisher Scientific, USA). In detail, 2 mL prepared Fe@OVA-IR820 was put into dialysis bags that could intercept molecular weight at 3500 Da (Yuanye, Shanghai, China). The dialysis bags were divided into two groups and soaked in 30 mL PBS buffer with pH values of 5.5 and 7.4, and kept shaking at 100 rpm in water bath at 37℃. At every time points of the time curve, 1 mL PBS solution was extracted as planned, then the absorbance was measured under 550 nm UV light (SP-756P, Shanghai Spectral Instrument Co., LTD). The concentration of released iron ions was calculated by using the method of iron colorimetric assay kit (Applygen, Beijing, China). After each extraction 1 mL isothermal medium was added into container timely.

Encapsulation efficiency (EE) and drug loading (DL) of Fe@OVA-IR820

The amounts of Fe and IR820 added to the system during the preparation of nanovaccine were recorded as W_{Fe-1} and $W_{IR820-1}$. Recorded the weight of prepared samples as W_1 after lyophilization. Then nanoparticles of a certain quality (W_2) was measured and dissolved, then the OVA content was detected by BCA kit (Beyotime, Shanghai, China). Ultraviolet absorption scanned spectrogram of solution to acquire OD value, which was converted to calculate concentration of IR820 to obtain OVA weight (W_{OVA}) and IR820 weight (W_{IR820}) severally. The weight of $Fe(OH)_3$ was measured by $W_{Fe(OH)3} = W_2 - W_{OVA} - W_{IR820}$. Ultimately, the EE and DL of each substance can be calculated:

$$\mathrm{EE\%\ of\ Fe(OH)_3} = \frac{W_{Fe(OH)_3} \times \frac{W_1}{W_2} \times \frac{Mr_{Fe}}{Mr_{Fe(OH)_3}}}{W_{Fe\text{-}1}} \times 100\%$$

1

$$\mathrm{EE\%\ of\ IR820} = \frac{W_{IR820} \times \frac{W_1}{W_2}}{W_{IR820\text{-}1}} \times 100\%$$

2

$$\mathrm{DL\%\ of\ Fe(OH)_3} = \frac{W_{Fe(OH)_3}}{W_2} \times 100\%$$

3

$$\mathrm{DL\%\ of\ IR820} = \frac{W_{IR820}}{W_2} \times 100\%$$

4

Evaluation of photothermal performance

Fe@OVA-IR820 nanovaccine and free IR820 were dissolved at gradient concentrations (5, 10, 20, 50 μg/mL, calculated by IR820) and irradiated with a power density of 2.5 W/cm^2 (808 nm, 10 min), using near-infrared laser emitted from infrared fiber laser (Leoptics, Shenzhen, China). Infrared thermal imager (Fotric 225) was employed to collect temperature of the solution.

Detection of glutathione consumption and proficiency test of extracellular ·OH

Under the condition of pH 8.0, phthalaldehyde and GSH can react to produce fluorescent substances. 18 mL OVA, Fe@OVA, Fe@OVA-IR820 solutions (5 μg/mL, calculated by IR820) was respectively mixed with 1 mL GSH solution (2 mM). Then 1 mL phthalaldehyde ethanol solution (8 mg/mL) was instilled. After blending and incubating for 20 min murkily, fluorescence value of different groups was measured (340 nm excitation and 430 nm emission) by multi-functional microplate analyzer (Tecan Infinite F200, Tecan, Switzerland). The GSH content was described as the ratio of the relative content with the blank group.

In addition, intracellular GSH concentration was determined by GSH and GSSG detection kit (Beyotime, Shanghai, China). B16-OVA cells were incubated with OVA, Fe@OVA, Fe@OVA-IR820, Fe@OVA-IR820 + NIR (5 μg/mL, calculated by IR820) for 24 h after which procedure the Fe@OVA-IR820 + NIR group was irradiated for 5 min (808 nm, 2.5 W/cm^2). Without nanoparticles cells were used as control. Cellular glutathione levels were then measured according to product specifications. The relative level of glutathione content in treatment group was calculated by comparing with control group.

Crystal violet can be discolored by hydroxyl radicals generated by decomposition of hydrogen peroxide. This experimental process can be used to verify whether Fe@OVA nanoparticles can catalyze the formation of hydroxyl radicals. The crystal violet solution was mixed with hydrogen peroxide and Fe@OVA, which was left at room temperature for 1 hour. Crystal violet and hydrogen peroxide as control group and all samples were scanned by UV-vis spectroscopy.

Cellular uptake and distribution

B16-OVA cells were inoculated for one day to make adherence. After, the cell medium was added with Fe@OVA-IR820 and free IR820 (5 μg/mL, calculated by IR820) for 2, 4, 8, 12 h. Later rinsed B16-OVA cells with PBS and cultured them with 1 mL DMEM medium containing lysosome probe (50nM) at 37℃ for 30 min. After swilling and immobilization, DAPI was used for staining B16-OVA cells for 15 min, followed by observation of laser scanning confocal microscope (LSCM) (Leica, Wetzlar, Hesse, Germany). "ImageJ" software was used to quantitative test mean intracellular fluorescence intensity.

In vitro cytotoxicity assay

After culturing for one day, the medium of B16-OVA cells (overexpressing OVA) was exchanged to 200 μL Fe@OVA-IR820 NPs and IR820 DMEM medium with the following concentrations: 0.1, 0.2, 0.5, 1, 2, 5

μg/mL (calculated by IR820), and then the cells were incubated for another 24h. Irradiated half of the orifice plate for 5 minutes (808nm, 2.5 W /cm^2). The relative viability of B16-OVA was assessed through MTT method (n = 5).

To certify the occurrence and effect of ferroptosis, B16-OVA cells were added to blank medium and medium mixed with OVA, Fe@OVA, Fe@OVA-IR820 (5 μg/mL, calculated by IR820). Each parallel group was added with different related-pathway inhibitors, including DFO (62.5 μM after mixing), Fer-1 (50 nM after mixing), VE (12.5 μM after mixing) and GSH (2.5 mM after mixing). All groups were incubated for one day and MTT method was used to assess relative viability of B16-OVA (n = 5).

In vitro validation of markers related to ferroptosis pathway induced by nanovaccine

B16-OVA cells were exposed blank medium, OVA, Fe@OVA, Fe@OVA-IR820 (5 μg/mL, calculated by IR82) for 6 h after seeded into 6-well plates for one day. Irradiated half of holes containing Fe@OVA-IR820 5 minutes (808 nm, 2.5 W/cm^2). DCFH-DA (Beyotime, Shanghai, China) staining method was applied to detect intracellular ROS levels and BODIPY$^{581/591}$-C11 (Thermo, Waltham, MA) could be used as an LPO sensor to detect intracellular LPO level[34]. The B16-OVA cells were stained with ROS sensor (10 μM) after the cell fragments were cleaned by PBS to detect intracellular ROS production. The dye could be changed to LPO sensor (5 μM) and incubated for 20 min to detect LPO production. After staining and washing, B16-OVA cells were observed under LSCM.

Analyzation of GPX4 and detection of intracellular H_2O_2 level

Western blotting was chosen to evaluate GPX4 levels. B16-OVA cells were cleaved on ice with NP40 lysis buffer containing 0.1% protease inhibitor cocktail after treated with different groups (5 μg/mL, calculated by IR820) and the above methods. The cytoplasmic proteins collected by centrifugation after lysis were boiled to degenerate, followed by electrophoresis in 12% SDS-PAGE Bis-Tris Gel (Invitrogen, Carlsbad, CA), and then transferred onto nitrocellulose membranes with 0.22 μm pores. 5% skim milk powder was prepared to soak and wash the membranes. Then membranes were sequentially incubated with primary antibodies of β-actin (Beyotime, Shanghai, China) or GPX4 (Absin, Shanghai, China) and corresponding fluorescent secondary antibodies. Images were collected by chemiluminescence method and analyzed by "ImageJ" software.

Micro hydrogen peroxide detection kit (Solarbio, Beijing, China) was employed to detect. After incubating with nanovaccines for 24 h, and half of holes containing Fe@OVA-IR820 were irradiated for 5 minutes (808 nm, 2.5 W/cm^2). Blank medium cells without nanoparticles were added as control. B16-OVA cells were gathered and put into ultrasonic cell breaker to crush. After operation, transferred treated cells and measured the absorbance value at 415 nm.

Detection of immunogenic cell death intracellular biomarkers

ATP detection kit (Beyotime, Shanghai, China) was used to measure ATP content in cells. B16-OVA cells were incubated Fe@OVA-IR820, Fe@OVA-IR820 and ferrostatin-1. Cells without nanoparticles treatment were added as control. Half of holes containing Fe@OVA-IR820 were irradiated for 5 minutes (808 nm, 2.5 W/cm^2). Lysate was added at the ratio of one-tenth of the amount of cell culture medium, and lysate cells were operated on ice. The RLU value of supernatant collected by centrifuge was detected by luminomete. In order to eliminate the effect of protein concentration, the intracellular total protein amount was determined to more accurately display the released ATP concentration.

B16-OVA cells were exposed to OVA、Fe@OVA and Fe@OVA –IR820 (5 μg/mL, calculated by IR820)for 12 h, and half of the Wells (808 nm, 2.5 W /cm^2) containing Fe@OVA-IR820 were irradiated for 5 minutes. The control group was added blank cell medium without nanoparticles. After treatment, 4% paraformaldehyde was added for cell immobilization. Followed by cleaning with PBS again, corresponding primary antibody of calreticulin (Beyotime, Shanghai, China) and high-mobility group box 1 (Absin, Shanghai, China) were added and placed overnight at 4℃. After staining with Alexa 488 labeled secondary antibody and washing, B16-OVA cells were observed under LSCM.

Detection of nanovaccine-uptake by dendritic cells

After the C57BL/6 mice (6-8weeks) were sacrificed, removed their femur and tibia in a sterile environment, and rinsed with 75% alcohol, PBS and RPMI 1640 full medium in sequence. Washed the bone marrow cavity with 1–2 mL full medium repeatedly for each bone to collect cells. After centrifugation of the obtained bone marrow cells to collect and lyse the red blood cells in the bone marrow, they were collected through a 74 um filter membrane. The BMDCs were seeded on a 10 mm sterile petri dish. The culture suspension was gently sucked to evenly mix cells when reached the sixth day, and the collection was centrifuged to discard the supernatant. After suspending and incubating with IR820 and Fe@OVA-IR820 for 4 hours, flow cytometry (LSRFortessa, BD, USA) and confocal microscopy were used to evaluate the entry of nanovaccine into dendritic cells.

Induction of dendritic cell maturation in vitro

After 7 days of culturing, dendritic cells were transferred from a 10 mm sterile petri dish to a sterile 6-well plate. B16-OVA cells were inoculated with Fe@OVA-IR820 and Fe@OVA-IR820 + ammonium glycyrrhizinate (0.2 mg/mL) for 12 h respectively. Half of the holes added with Fe@OVA-IR820 were irradiated with 808 nm laser (2.5 W/cm^2) for 5 min, and cultured to collect damaged debris, which were then added to the BMDCs in the 6-well plate.

Dendritic cells after 7 days of culturing were exposed to 5 μg/mL (calculated by IR820) OVA, Fe@OVA, Fe@OVA-IR820 for 24 h. Dendritic cells were dyed by fluorescent antibodies against CD11c, CD80 and CD86. Flow cytometry (Becton, Franklin, USA) was used detect and analyze.

Anti-tumor experimental model construction of C57BL/6 mice

When B16-OVA cells grew to 2.5×10^5 cells/well, they were collected with 100μL PBS solution and transplanted subcutaneously (s.c.) into the right back of male C57BL/6 mice aged 6–8 weeks to establish a melanoma model as the primary tumor. Four days after the initial inoculation, a second tumor was seeded contralateral as an artificial analog of metastasis. All laboratory mice were randomly divided into 6 groups (n = 5) :(1) Control; (2) OVA; (3) Fe@OVA; (4) Fe@OVA-IR820; (5) Fe@OVA-IR820 + NIR; (6) Fe @ OVA - IR820 + NIR + CTLA-4. Three days later, when the primary tumors of B16 grown on C57BL/6 mice had reached about 200 mm^3, 50μL of the nanoagent was intratumoral injected into these tumors (~ 5 μg/mL, calculated by IR820). Two hours later, tumors (right) injected with nanovaccines in groups Fe@OVA-IR820、Fe@OVA-IR820 + NIR、Fe@OVA - IR820 + NIR + CTLA-4 were exposed to laser 10 min for radiation therapy (808nm, 2.5 W/cm^2) at 3-minute intervals of 2 minutes. PBS injection group was the control group. This point in time was defined as day 0. Gave the medicine every two days. On days 2, 5, 8, 11 and 14, anti-CTLA-4 antibody was intraperitoneally (i.p.) injected at a dose of 2.0 mg/kg. The weight and tumor volume of each mouse were noted during therapy. Tumor volume could be estimated by the following equation:

$$\text{Tumor volume}=\frac{\text{Length}\times\text{Width}^2}{2}$$

5

The mice were euthanized after two weeks. Paraffin was chosen to embed extracted tumors and organs for hematoxylin and eosin (H&E) staining. The observation was under upright microscope (BX63, Olympus, Japan). The lungs of different treatment groups were soaked in Bouin's solution for 24 hours to record pulmonary metastasis of melanoma.

Enhanced antitumor immune responses

Tumor was dehydrated with sucrose and were prepared to develop frozen sections. To explore changes in immune level induced by vaccine treatment in vivo, the content of calreticulin (CRT) and high-mobility group box 1 (HMGB1) in tumor tissues were monitored by immunofluorescence staining. Besides, lymph nodes of mice were removed and the maturation of DCs was analyzed with comparation. Tumor, spleen and lymph node were removed from the mouse cadaver, ground with 70mm filter and washed. Followed instructions of animal tumor infiltrating tissue lymphocyte separation fluid kit (Solarbio, Beijing, China) to separate and purify the lymphocytes in the tumor tissue. Fluorescein - coupled antibodies were used to dye individual cells. The staining regimen for dendritic cells was the same as in vitro to make dyed cell suspension. Intratumoral infiltration of CD8 + T cells and splenic CD4/CD8 + T cells was detected and compared by flow cytometry. Besides, purified lymphocytes were collected from the tumor to detect and analyze the NK cell activation in the tumor. The collected cells were dyed with CD3e and NKp46 antibody

(Becton, Franklin, USA) then measured by flow cytometry. All samples were analyzed using FlowJo software.

The excised tumor tissue was treated with ultrasonic cell fragmentation instrumen to obtain individual tumor cells. The levels of interferon γ (IFN-γ), tumor necrosis factor α (TNF-α) and interleukin 6 (IL-6) were measured by enzyme-linked immunosorbent assay (ELISA). Tumor samples of each group were prepared according to instructions and determined according to ELISA kit protocol.

Statistical analysis

All assays ($n \geq 3$) were expressed as mean ± SD. Prism 8.0 (GraphPad, USA) was used for data analysis and visualization utilizing one-way analysis of variance (ANOVA). If $P < 0.05$ (*$P < 0.05$, **$P < 0.01$, ***$P < 0.001$), the difference between groups was marked as statistically significant.

Results And Discussion

Characterization of Fe@OVA-IR820 nanovaccine

Deionized water was used to dissolve OVA. Then the solution was added with ferric chloride solution drop by drop to develop the Fe@OVA nanoparticles through metal cation chelation by frontal amino acid residues in the central of OVA. The system pH value was converted into 12 and held for 2 hours to form the rapid accumulation of ferric hydroxide in-situ. Then the pH value was changed to 4 for scavenging denatured protein. The isoelectric point of OVA is 4.5 and metallic cations are positively charged, so the Fe@OVA nanoparticles should be positive at this pH. After instillation of IR820 solution, IR820 molecules were attached to the nanoparticles by electrostatic adsorption to develop Fe@OVA-IR820 nanovaccine. Free IR820 was eliminated by centrifugation followed by ultrafiltration.

Fe@OVA and Fe@OVA-IR820 were all showed had stable and uniform mean sizes of 168.2 ± 6.50nm and 155.3 ± 1.50nm respectively **(Fig. S1**), in which cases the polydispersion index was both below 0.25. Due to electrostatic compression, the particle diameter of Fe@OVA-IR820 in aqueous solution will be slightly smaller than Fe@OVA. The ζ-potential of Fe@OVA and Fe@OVA-IR820 were respectively 7.92 ± 0.96 mV and − 3.19 ± 0.86 mV (**Fig. S2**). The stability of nanoparticles was satisfied during 14 days (**Fig. S3**). Transmission electron microscopy showed that both types of prepared nanoparticles had clear spherical appearance and uniform size (Fig. 1B). Given that the main body of the nanovaccine was protein, it was reasonable that the kinetic diameter of the nanovaccine in an aqueous solution was slightly larger than that in the vacuum compression state when the transmission electron microscope was working. Because of the accumulation of IR820 in the outer layer, the actual diameter of Fe@OVA-IR820 particles is larger than Fe@OVA at this time. Then we detected the IR820 by UV scanning (Fig. 1C), and the image showed an absorption peak at 685 nm, revealing the successful loading of IR820. Nanovaccines were consistent with their desired photothermal properties based on the feedback of the infrared thermal imager, showing excellent photothermal conversion (Fig. 1D). As it could be seen from **Fig. S4 A** and **Fig. S4 C**, the intensity of time thermal effect was positively correlated with irradiation time and concentration of

nanoparticles at the same laser power. Irradiation at 808nm for 10 min increased the temperature of 50 μg/mL Fe@OVA-IR820 by 39.1℃ (**Fig. S4 B**), which was close to the 36℃increased after irradiation with 50μg/mL IR820 solution for 10 min (**Fig. S4 B**).

The release of iron ions from nanovaccine was investigated **(**Fig. 1E**)**. The cumulative release of iron ions in the preparation reached 84.9% after 72 hours at pH 5.0, compared with 41.7% after 72 hours at pH 7.0, which was almost half of the former. It could be inferred that Fe@OVA-IR820 nanovaccine was able to effectively and continuously release iron ions in slightly acidic tumor microenvironment and tumor cells. The release of ferric iron contained by Fe@OVA-IR820 contains could consume the GSH at the tumor site (Fig. 1F). The GSH concentration decreased significantly after treatment with preparations containing ferric iron when compared with the control group. Slight decrease in OVA group might be due to the reducing action of disulfide bonds in OVA. Fe^{3+} could react GSH at the tumor site and was converted to produce Fe^{2+}, which was more effective to catalyze Fenton reaction[35], and reacted with hydrogen peroxide in tumor tissue to produce hydroxyl radical with strong oxidation. We chose crystal violet to detect hydroxyl radicals produced in Fenton reaction. The chemical structure of crystal violet could be destroyed by hydroxyl radical (•OH) with strong oxidability and the solution was discolored concurrently[36], hence the peroxidase-like ability of nanovaccine was verified by crystal violet chromogenic experiment (Fig. 1G). Only after the addition of nano-preparation, the crystal violet characteristic peak at 585nm disappeared, convincingly indicating the formation of hydroxyl radical. As the circular dichroism experiment in Fig. 1H, the secondary structure of OVA proteins in Fe@OVA and Fe@OVA-IR820 did not change significantly after preparation, therefore the basic biological functions of ovalbumin were still played normally.

In vitro celluar uptake, cytotoxicity, and Ferroptosis pathway validation

Effective intracellular tumor accumulation of nanovaccines is required for therapeutic effect, so we evaluated their ability to be internalized by cells in vitro. After incubating with nanovaccine and free IR820 for different periods, and the images of B16-OVA cellular uptake were investigated by LSCM. It was evident that the intracellular cumulation of nanovaccine gradually increased over time, while the cumulative uptake concentration of free photothermal agent (IR820) did not change significantly over time (Fig. 2A). During the first 4 hours of co-incubation, cells in the free IR820 group accumulated more, which was gradually exceeded by intracellular accumulation in the Fe@OVA-IR820 nanovaccine group within 8 to 12 hours of administration, which is consistent with previous report[37]. This pathway may help explain the Fe@OVA-IR820 the increased ability of nanovaccine to internalize IR820 into cancer cells.

The cytotoxicity of the nanovaccine against B16-OVA cells was tested in standard MTT cell viability assays (Fig. 2B) and showed no significant cytotoxicity at low concentrations without laser irradiation, indicating remarkable biocompatibility. As the concentration of the preparation increased, ferroptosis enhanced cytotoxicity due to the introduction of iron element. Irradiation of the 808nm laser at 5 μg/mL

for 5 min in the Fe@OVA-IR820 group killed 78.54% of the cells, compared with the free IR820 killed only 60.21%, weakening by nearly 20%.

Ferroptosis, as one of regulated cell death forms, is motivated by GPX4 inactivation and ROS cumulation. In particular, lipid hydroperoxides accumulation acts a vital factor in this process[38]. GPX4 expression was showed in Fig. 2D and conducted semi-quantitative analysis of the gray image (Fig. 2E). It could be observed that the expression level of GPX4 protein in different preparation groups was decreased to some extent in the following order: Control > OVA > Fe@OVA ≈ Fe@OVA-IR820 > Fe@OVA-IR820 + NIR. Metabolism of intracellular lipid oxides was impaired due to GPX4 invalidation and occurred metabolic disturbance. Under the catalytic action of iron ions, Fenton reaction was amplified to produce excessive ROS, resulting in the accumulation of reactive oxygen free radicals on membrane lipids. Detection images taken by LSCM were shown in Fig. 3A. Photosensitivity IR820 generated heat and ROS[39] after irradiating with laser. Meanwhile, the ROS produced directly damage the tumor site and destroyed endosomes and lysosomes, thus promoting drug delivery to the nucleus, mitochondria and other targets in the cell[40]. Under near-infrared light, IR820 cooperated with iron ions to form synergy, increasing ROS level in Fe@OVA-IR820 + NIR group. Accumulation of LPO was one of the important factors contributing to ferroptosis[41]. Compared with the control group and OVA group, Fe@OVA, Fe@OVA-IR820 and Fe@OVA-IR820 + NIR groups showed stronger fluorescence signal (**Fig. S6**), strongly demonstrating the satisfactory ability of Fe@OVA-IR820 nanovaccine to induce ROS and LPO production in B16-OVA cells.

Intracellular redox imbalance caused by ferroptosis could be inhibited with addition of related inhibitors or iron-chelating agents[42]. It could be seen that cell viability was significantly increased after ferroptosis inhibitor Fer-1 and iron chelatord DFO was added to the medium (Fig. 3B), indicating that the ferroptosis pathway was effectively inhibited. The results showed the Fe@OVA-IR820 nanovaccine could effectively kill tumor cells mainly through ferroptosis. Supplementation of α -tocopherol, which has antioxidant properties[43], reduced intracellular ROS levels and significantly attenuated the cytotoxicity induced by Fe@OVA-IR820 nanovaccine. Figure 3C demonstrated the ability of nanovaccine to reduce the level of GSH in B16-OVA cells, which was performed through the process of Fe^{3+} reduced to Fe^{2+} by GSH. Hydrogen peroxide H_2O_2 was consumed in cells (Fig. 3D), which was agreed with in vitro results during Fenton reaction. GPX4 activity was inhibited with GSH reduction and thus promoting ferroptosis[44]. The addition of GSH could also alleviate the death rate of B16-OVA cells (Fig. 3B), which reversely confirmed the appearance of ferroptosis caused by Fe@OVA-IR820 nanovaccine. All these above data demonstrated that ferroptosis patterns play an important role in Fe@OVA-IR820 nanovaccine therapy.

ICD induction and antitumor immunogenicity elicitation cooperated with ferroptotic cell death

During immunogenic cell death program, ATP was released through exocytosis vesicles in an autophagy-dependent manner. ATP levels in cells treated with different preparation groups were evaluated by luminometry detection method[45]. As shown in Fig. 3E, B16-OVA cells could effectively release ATP after being treated with nanovaccine to initiate ICD process regardless of whether PTT occurred, while the

addition of Fer-1 was able to significantly inhibit this process, indicating that ferroptosis was the trigger for initiating ICD. The main cause was the increase of intracellular ROS after ferroptosis, which generated ICD[46]. Besides, CRT and HMGB1, common biomarkers of chemotherapy-induced ICD, were detected. LSCM examed that B16-OVA cells showed stronger fluorescence signal for CRT after preparation incubation, while HMGB1 in the nucleus showed a downward trend due to release out of the cell (**Fig. S7**). When the nanovaccine treatment was combined with 808nm NIR irradiation, more cells were seen to develop ICD. Constant NIR irradiation of cells produced hyperthermia for PTT with the ability to enhance ICD[17, 47, 48].

The tumor microenvironment was usually immunosuppressive. One important strategy in tumor immunotherapy was to overcome inhibitory immune microenvironment. ICD in microenvironment is needed to allow antigen-presenting cell(APC) cells to recruit, activate, and migrate to lymph nodes and tertiary lymphoid tissues for cross-presentation activation[49]. After extracellular released by exocytosis, ATP signal released a "find-me" signal to DC progenitors and macrophages, and myeloid cells were facilitated to recruit to active ICD sites. Tumor cells were promoted to be phagocytosed by DC cells with the “eat me” signal CRT exposed to serosal surface. Surface exposed CRT could bind to LRP1 on APC cell surface to activate both natural and adaptive immunity[49, 50]. B16-OVA cells released HMGB1 extracellular during this process, thereby activating signaling pathways and activating immunity[49, 51]. The experimental results obtained above once again confirm the ability of nanovaccine to effectively induce ICD.

In order to investigate whether the nanovaccine itself and the cell death induced by ICD and ferroptosis after its treatment could synergistically induce antitumor immunogenicity, an in vitro stimulation to promote maturation of DC cells was conducted (Fig. 4A**)**. First, extracted bone marrow-derived cells (BMDCs) of C57BL/6 mice at 6–8 weeks were treated with free IR820 and Fe@OVA-IR820 nanovaccine respectively. The uptake results of DCs in different treated groups was measured by different detection methods were exhibited in Fig. 4B and Fig. 4C. demonstrating that Fe@OVA-IR820 nanovaccine could enter cells. The experiment was then performed with two parallel groups. Extracted BMDCs were treated with OVA, Fe@OVA NPs and Fe@OVA-IR820 nanovaccine respectively, and the untreated group served as the control group (Fig. 4D). Afterwards, B16-OVA tumor cells were treated with blank medium, Fe@OVA-IR820 nanovaccine, Fe@OVA-IR820 nanovaccine with ammonium glycyrrhizinate, Fe@OVA-IR820 nanovaccine with 808nm laser respectively, and then the medium was added to the growth environment of BMDCs for stimulation. DCs were then dyed with fluorescent antibodies. The results shown in (Fig. 4E) revealed that the nanovaccine could significantly promote DC maturation. Figure 4G showed that the combination of Fe@OVA-IR820 nanovaccine and laser treatment significantly promoted DC maturation, which should be due to the promotion of DAMPs production and secretion of B16-OVA cells after treatment. As one kind of DAMPs, HMGB1 has been reported to promote DC maturation[52]. The addition of ammonium glycyrrhizinate (HMGB1 inhibitor) inhibited adaptive immune response[17], verifying the above proposed hypothesis. These results suggested that Fe@OVA-IR820 nanovaccine could induce an effective immune response by direct stimulation, whereas photothermal therapy could enhance this response by increasing the release of endogenous antigens after plasmatorrhexis due to heat.

Antitumor efficacy in vivo

After demonstrating that Fe@OVA-IR820 nanovaccine could fight tumors through multiple synergies, we then attempted to explore whether combination therapy based on Fe@OVA-IR820 nanovaccine could activate anti-tumor immune response after inducing ferroptosis patterns, and whether this strong immune response could achieve the goal of radical cure of tumor and prevent metastasis. In addition, multimodal treatment with CTLA-4 blockade combined with other therapies could efficaciously initiated immune responses targeted at tumor, thereby restraining tumor metastasis[53, 54]. Hence, the effect was explored in combination with CTLA-4 blocking treatment.

Figure 5A demonstrated B16-OVA subcutaneous tumor model establishment and treatment plan. Briefly, C57BL/6 mice with both primary and distal inoculated tumors were divided into six groups. Same dose of IR820 in the Fe@OVA-IR820 nanovaccine were injected during the treatment period. During the two-week treatment, tumors in control group were growing mushroomly, accompanied by a small range of weight gain, while the weight of mice in other groups showed no significant difference, which were around 25g (Fig. 5B). Growth curve in control and OVA group grew very rapidly for primary tumor. The iron-containing Fe@OVA, Fe@OVA-IR820, and Fe@OVA-IR820 + NIR groups inhibited tumor growth during the first two weeks after treatment, confirming the validity of ferroptosis and photothermal effects. The difference between every group was due to the depletion of intracellular GSH induced by ferroptosis, and the redox imbalance caused by ROS produced by IR820 after irradiation. Remarkably, the Fe@OVA-IR820 + NIR + CTLA-4 group showed the most significant tumor inhibition, with almost no growth in tumor volume (Fig. 5C), and some of the experimental mice tumor were cleared during treatment without recurrence (**Fig. S8**).

In this model, distal tumors did not receive direct treatment, but they were treated closely with a strong internal immune response that was stimulated by Fe@OVA-IR820 nanovaccine. It could be seen that Fe@OVA-IR820 + NIR group partially slowed tumor growth on both sides (Fig. 5D). The combination of PTT and CTLA-4 blockade based on Fe@OVA-IR820 not only almost thoroughly eliminated initial tumor, but also strongly inhibited distant tumor growth (Fig. S8), revealing the strong application potential of Fe@OVA-IR820 nanovaccine combination therapy.

After the completion of the treatment cycle, tumors were surgically removed, weighed and photographed (Fig. 5E, **Fig. S8**, and **Fig. S9**). H&E staining images showed the densest tumor growth in the control and OVA groups, while the remaining preparation groups were treated with nanovaccines that damaged the tumor and reduced cell proliferation (Fig. 5F). These images suggested that the combination among ferroptosis-induced immunotherapy based on Fe@OVA-IR820 nanovaccine, PTT therapy and CTLA-4 blockade could provide a powerful collaborative antitumor immune influence to inhibit tumor cell mushrooming. The next step was to explore the ability of Fe@OVA-IR820 to prevent systemic metastasis by counting metastatic tumor foci (Fig. 5G). The combination among Fe@OVA-IR820, photothermal and immune checkpoint inhibitors resulted in the least number in lung metastases compared to control group, indicating the excellent function of Fe@OVA-IR820 nanovaccine in inhibiting tumor metastasis.

Immune response induced by Fe@OVA-IR820 nanovaccine in vivo

The exposure of the ICD biomarker CRT and HMGB1 were detected to verify the consistent ability of Fe@OVA-IR820 nanovaccine to prompt ICD in vitro and in vivo. Ferroptosis stimulated ICD was enhanced in Fe@OVA group and Fe@OVA-IR820 group when compared to control (Fig. 6A). Exposure of CRT and HMGB1 in Fe@OVA-IR820 + NIR group and Fe@OVA-IR820 + NIR + CTLA-4 group were significantly increased, indicating that PTT has a stronger ability to enhance ICD[47] effect with ferroptosis. Assessment of DC maturation in draining lymph nodes and tumors were shown in Fig. 6B and Fig. 6C. Obviously, the proportion sequence of CD11c + CD80 + CD86 + mature DC in these two parts was shown as: Fe@OVA-IR820 + NIR + CTLA-4 > Fe@OVA-IR820 + NIR > Fe@OVA-IR820 > Fe@OVA > OVA > Control. The increasing proportion of DC cell maturation demonstrated that Fe@OVA-IR820 nanovaccine could be used to induce an effective mode of immunoenhancement through ferroptosis, which could be amplified by the addition of PTT with immune checkpoint inhibitors. Beyond that, increasing splenic helper CD4 + and cytotoxic CD8 + T cells (Fig. 6D) also strongly supported the enhanced immune response in the nanovaccine treated model.

Flow cytometry showed that the combination therapy of Fe@OVA-IR820 + NIR + CTLA-4 group effectively promoted intratumoral natural killer (NK) cells (Fig. 7A) and cytotoxic T lymphocytes (Fig. 7B). These cells are likely to be important effector cells for controlling tumor regression and metastasis[55]. Significantly higher levels of intratumor NK cells were observed in the different groups injected with Fe@OVA-IR820 nanovaccine, while there was only 6.25% in control group and 8.25% in OVA group. A similar trendency was displayed in cytotoxic CD8 + T cells. ELISA test kit was used to detect immuno-related cytokines, including IFN- γ (Fig. 7C) that led to tumor extinction[56], TNF-α (Fig. 7D) that played a crucial role in immune function[57], and IL 6[58, 59] (Fig. 7E) that induced by the raising of matured DC. IFN-γ and TNF-α are also representative markers of tumor maturation immunogenesis reported[50, 58, 60]. ELISA results showed that the treatment stimulation of Fe@OVA-IR820 nanovaccine could effectively promote the expression and release of tumor immune-related cytokines. The group that received the Fe@OVA-IR820 + NIR combination had expressed significantly higher levels of cytokine than the others, further illustrating and verified that the combination immunotherapy induced by ferroptosis induced by nanovaccine achieved the most effective tumor suppression.

Throughout the treatment period, a strong immune response was triggered after the nanovaccine injected into the tumor. After uptaken by tumor cells, Fe@OVA-IR820 eliminated GSH by releasing iron ions and induced the initiation of Fenton reation to produce ROS, resulting in ferroptpsis and ICD. The photothermal effect of IR820 was used to accelerate the release of ferric ion and amplify the antitumor effect of ferroptpsis[61]. Meanwhile, the nanovaccine with photothermal effect was irradiated by 808 nm NIR to generate heat that could enhance ICD consequence, which attested by the release of CRT and HMGB1 detected by immunohistochemical photographs. Tumor-related antigens released after the nanovaccine-stimulated death of cancer cells and led to DC maturation, synchronously stimulated the

immunogenicity for cancer immunotherapy[62]. Antigen was presented from DC to CD8 + T cells, moreover multiple treatments also improved tumor NK cells, which helped promote CD8 + T cells to retard tumor growth[55]. The significant increase of TNF-α, IFN-γ and IL-6 in Fe@OVA-IR820 + NIR + CTLA-4 group of combination therapy exhibited that the treatment of melanoma with NIR-triggered ferroptosis-inducing nanovaccine based on biomineralized ovalbumin in combination with checkpoint blockade could satisfactorily reverse the immunosuppressive environment and achieve the desired therapeutic effect. Collected tunnel images further verified the excellent synergistic antitumor effect of Fe@OVA-IR820 nanovaccine combination therapy. These results certified that the combination therapy centering on ferroptosis-induced nanovaccine could be used as a reference for future cancer treatment.

Conclusions

Here, we constructed a photothermal nanovaccine inducing-ferroptosis based on biomineralized ovalbumin with checkpoint blockade for melanoma therapy which could strongly inhibit tumor growth and autonomously treat metastatic tumors through enhanced immune response. The Fe@OVA-IR820 nanovaccine is simple and feasible to prepare without chemical contamination, can be used for NIR-induced PTT, and has successfully treated primary and metastatic melanoma with combined CTLA-4 blockade. Fe@OVA-IR820 nanovaccine promoted Fenton reaction by releasing iron ion to consume GSH, down-regulating GPX4 expression and producing excessive ROS, and promoted ferroptosis. The ferroptosis process induced by nanovaccine therapy initiated a powerful immune response in vivo, which is enhanced by PTT, together catalyzed the generation of systemic anti-tumor immune responses to achieve therapeutic goals. We proved that Fe@OVA-IR820 nanovaccine has great potential to achieve extraordinary synergistic therapeutic effects in banishing initial tumors and curbing distant ones. In conclusion, this simple and readily available nanovaccine supplied a common strategy for flexible combinations in biomedical applications, and the superior therapeutic efficacy of the treatment makes this platform promising for anticancer therapy.

Declarations

Acknowledgements

The authors greatly appreciate the help from the school of pharmacy of Shanghai Jiao Tong University,

Authors's contributions

Siyu Ma: Ideas; formulation or evolution of overarching research goals and aims.

Jie Yang: Conducting a research and investigation process, specifically performing the experiments.

Tianxu Fang: Development or design of methodology; creation of animal models.

Jun Zhang: Preparation, creation and presentation of the published work. Acquisition of the financial support for the project leading to this publication.

Xiuhua Pan: Contributed to the conception of the study;

Yawen Wei: Provision of study materials.

Ning Yang: Helped perform the analysis with constructive discussions

Zengyi Liu: Contributed significantly to analysis

Qi Shen: Acquisition of the financial support for the project leading to this publication.

Funding

This work was supported by grants from the National Natural Science Foundation of China (Grant No. 81972812) and Shanghai Jiao Tong University “Starting Program for Young New Teachers” (Project No. 20X100040060).

Availability of data and materials

All data generated or analysed during this study are included in this published article (and its supplementary information files).

Ethics approval and consent to participate

All animal experiment procedures in this research were carried out under the approval of the Institutional Committee for Animal Care and Use (IACUC) of Shanghai Jiao Tong University (approval number: A2018054).

Competing interests

The authors declare no competing financial interest.

Consent for publication

All authors agree to be published.

References

1. Ferlay J, Colombet M, Soerjomataram I, Mathers C, Parkin DM, Pineros M, Znaor A, Bray F: **Estimating the global cancer incidence and mortality in 2018: GLOBOCAN sources and methods**. Int J Cancer 2019, **144**:1941–1953.
2. Cong Y, Xiao H, Xiong H, Wang Z, Ding J, Li C, Chen X, Liang XJ, Zhou D, Huang Y: **Dual Drug Backboned Shattering Polymeric Theranostic Nanomedicine for Synergistic Eradication of Patient-**

Derived Lung Cancer. Adv Mater 2018, **30**.

3. Yang S, Tang Z, Hu C, Zhang D, Shen N, Yu H, Chen X: **Selectively Potentiating Hypoxia Levels by Combretastatin A4 Nanomedicine: Toward Highly Enhanced Hypoxia-Activated Prodrug Tirapazamine Therapy for Metastatic Tumors**. Adv Mater 2019, **31**:e1805955.
4. Luo L, Zhu C, Yin H, Jiang M, Zhang J, Qin B, Luo Z, Yuan X, Yang J, Li W, et al: **Laser Immunotherapy in Combination with Perdurable PD-1 Blocking for the Treatment of Metastatic Tumors**. ACS Nano 2018, **12**:7647–7662.
5. Park CG, Hartl CA, Schmid D, Carmona EM, Kim HJ, Goldberg MS: **Extended release of perioperative immunotherapy prevents tumor recurrence and eliminates metastases**. Sci Transl Med 2018, **10**.
6. Milling L, Zhang Y, Irvine DJ: **Delivering safer immunotherapies for cancer**. Adv Drug Deliv Rev 2017, **114**:79–101.
7. Hiller JG, Perry NJ, Poulogiannis G, Riedel B, Sloan EK: **Perioperative events influence cancer recurrence risk after surgery**. Nat Rev Clin Oncol 2018, **15**:205–218.
8. Hanci D, Sahin E, Muluk NB, Cingi C: **Immunotherapy in all aspects**. European Archives of Oto-Rhino-Laryngology 2016, **273**:1347–1355.
9. Iwai Y, Ishida M, Tanaka Y, Okazaki T, Honjo T, Minato N: **Involvement of PD-L1 on tumor cells in the escape from host immune system and tumor immunotherapy by PD-L1 blockade**. Proc Natl Acad Sci U S A 2002, **99**:12293–12297.
10. Rivalland G, Loveland B, Mitchell P: **Update on Mucin-1 immunotherapy in cancer: a clinical perspective**. Expert Opinion on Biological Therapy 2015, **15**:1773–1787.
11. Smith TT, Moffett HF, Stephan SB, Opel CF, Dumigan AG, Jiang XY, Pillarisetty VG, Pillai SPS, Wittrup KD, Stephan MT: **Biopolymers codelivering engineered T cells and STING agonists can eliminate heterogeneous tumors**. Journal of Clinical Investigation 2017, **127**:2176–2191.
12. Wang Q, Tian L, Xu J, Xia B, Li J, Lu F, Lu X, Wang W, Huang W, Fan Q: **Multifunctional supramolecular vesicles for combined photothermal/photodynamic/hypoxia-activated chemotherapy**. Chem Commun (Camb) 2018, **54**:10328–10331.
13. Wang Q, Dai Y, Xu J, Cai J, Niu X, Zhang L, Chen R, Shen Q, Huang W, Fan Q: **All-in-One Phototheranostics: Single Laser Triggers NIR-II Fluorescence/Photoacoustic Imaging Guided Photothermal/Photodynamic/Chemo Combination Therapy**. Advanced Functional Materials 2019, **29**.
14. Wang Q, Zhang P, Xu J, Xia B, Tian L, Chen J, Li J, Lu F, Shen Q, Lu X, et al: **NIR-Absorbing Dye Functionalized Supramolecular Vesicles for Chemo-photothermal Synergistic Therapy**. ACS Applied Bio Materials 2018, **1**:70–78.
15. Dobrovolskiene N, Pasukoniene V, Darinskas A, Krasko JA, Zilionyte K, Mlynska A, Gudleviciene Z, Miseikyte-Kaubriene E, Schijns V, Lubitz W, et al: **Tumor lysate-loaded Bacterial Ghosts as a tool for optimized production of therapeutic dendritic cell-based cancer vaccines**. Vaccine 2018, **36**:4171–4180.

16. Zhang X, Wang C, Wang J, Hu Q, Langworthy B, Ye Y, Sun W, Lin J, Wang T, Fine J, et al: **PD-1 Blockade Cellular Vesicles for Cancer Immunotherapy**. Adv Mater 2018, **30**:e1707112.
17. Ma Y, Zhang Y, Li X, Zhao Y, Li M, Jiang W, Tang X, Dou J, Lu L, Wang F, Wang Y: **Near-Infrared II Phototherapy Induces Deep Tissue Immunogenic Cell Death and Potentiates Cancer Immunotherapy**. ACS Nano 2019, **13**:11967–11980.
18. Zhu GZ, Lynn GM, Jacobson O, Chen K, Liu Y, Zhang HM, Ma Y, Zhang FW, Tian R, Ni QQ, et al: **Albumin/vaccine nanocomplexes that assemble in vivo for combination cancer immunotherapy**. Nature Communications 2017, **8**.
19. Melero I, Gaudernack G, Gerritsen W, Huber C, Parmiani G, Scholl S, Thatcher N, Wagstaff J, Zielinski C, Faulkner I, Mellstedt H: **Therapeutic vaccines for cancer: an overview of clinical trials**. Nat Rev Clin Oncol 2014, **11**:509–524.
20. Wang K, Wen S, He L, Li A, Li Y, Dong H, Li W, Ren T, Shi D, Li Y: **"Minimalist" Nanovaccine Constituted from Near Whole Antigen for Cancer Immunotherapy**. ACS Nano 2018, **12**:6398–6409.
21. Irvine DJ, Hanson MC, Rakhra K, Tokatlian T: **Synthetic Nanoparticles for Vaccines and Immunotherapy**. Chem Rev 2015, **115**:11109–11146.
22. Kuai R, Ochyl LJ, Bahjat KS, Schwendeman A, Moon JJ: **Designer vaccine nanodiscs for personalized cancer immunotherapy**. Nat Mater 2017, **16**:489–496.
23. Liu J, Tian L, Zhang R, Dong Z, Wang H, Liu Z: **Collagenase-Encapsulated pH-Responsive Nanoscale Coordination Polymers for Tumor Microenvironment Modulation and Enhanced Photodynamic Nanomedicine**. ACS Appl Mater Interfaces 2018, **10**:43493–43502.
24. Dixon SJ, Lemberg KM, Lamprecht MR, Skouta R, Zaitsev EM, Gleason CE, Patel DN, Bauer AJ, Cantley AM, Yang WS, et al: **Ferroptosis: an iron-dependent form of nonapoptotic cell death**. Cell 2012, **149**:1060–1072.
25. Yang WS, SriRamaratnam R, Welsch ME, Shimada K, Skouta R, Viswanathan VS, Cheah JH, Clemons PA, Shamji AF, Clish CB, et al: **Regulation of ferroptotic cancer cell death by GPX4**. Cell 2014, **156**:317–331.
26. Cao JY, Dixon SJ: **Mechanisms of ferroptosis**. Cell Mol Life Sci 2016, **73**:2195–2209.
27. Xie Y, Hou W, Song X, Yu Y, Huang J, Sun X, Kang R, Tang D: **Ferroptosis: process and function**. Cell Death Differ 2016, **23**:369–379.
28. Reyes-Ruiz A, Calvillo-Rodriguez KM, Martinez-Torres AC, Rodriguez-Padilla C: **The bovine dialysable leukocyte extract IMMUNEPOTENT CRP induces immunogenic cell death in breast cancer cells leading to long-term antitumour memory**. Br J Cancer 2021, **124**:1398–1410.
29. Jiang Q, Wang K, Zhang X, Ouyang B, Liu H, Pang Z, Yang W: **Platelet Membrane-Camouflaged Magnetic Nanoparticles for Ferroptosis-Enhanced Cancer Immunotherapy**. Small 2020, **16**:e2001704.
30. Zhang D, Zhang J, Li Q, Tian H, Zhang N, Li Z, Luan Y: **pH- and Enzyme-Sensitive IR820-Paclitaxel Conjugate Self-Assembled Nanovehicles for Near-Infrared Fluorescence Imaging-Guided Chemo-Photothermal Therapy**. ACS Appl Mater Interfaces 2018, **10**:30092–30102.

31. Zitvogel L, Kepp O, Senovilla L, Menger L, Chaput N, Kroemer G: **Immunogenic tumor cell death for optimal anticancer therapy: the calreticulin exposure pathway**. Clin Cancer Res 2010, **16**:3100–3104.
32. Wang Y, Yang T, Ke H, Zhu A, Wang Y, Wang J, Shen J, Liu G, Chen C, Zhao Y, Chen H: **Smart Albumin-Biomineralized Nanocomposites for Multimodal Imaging and Photothermal Tumor Ablation**. Adv Mater 2015, **27**:3874–3882.
33. Xie C, Cen D, Ren Z, Wang Y, Wu Y, Li X, Han G, Cai X: **FeS@BSA Nanoclusters to Enable H2S-Amplified ROS-Based Therapy with MRI Guidance**. Adv Sci (Weinh) 2020, **7**:1903512.
34. Wang SF, Li FY, Qiao RR, Hu X, Liao HR, Chen LM, Wu JH, Wu HB, Zhao M, Liu JN, et al: **Arginine-Rich Manganese Silicate Nanobubbles as a Ferroptosis-Inducing Agent for Tumor-Targeted Theranostics**. Acs Nano 2018, **12**:12380–12392.
35. Bolobajev J, Trapido M, Goi A: **Interaction of tannic acid with ferric iron to assist 2,4,6-trichlorophenol catalytic decomposition and reuse of ferric sludge as a source of iron catalyst in Fenton-based treatment**. Applied Catalysis B-Environmental 2016, **187**:75–82.
36. Fan HJ, Huang ST, Chung WH, Jan JL, Lin WY, Chen CC: **Degradation pathways of crystal violet by Fenton and Fenton-like systems: condition optimization and intermediate separation and identification**. J Hazard Mater 2009, **171**:1032–1044.
37. Zhu Y, Xue J, Chen W, Bai S, Zheng T, He C, Guo Z, Jiang M, Du G, Sun X: **Albumin-biomineralized nanoparticles to synergize phototherapy and immunotherapy against melanoma**. J Control Release 2020, **322**:300–311.
38. Yang WS, Stockwell BR: **Ferroptosis: Death by Lipid Peroxidation**. Trends Cell Biol 2016, **26**:165–176.
39. Hu D, Zhang J, Gao G, Sheng Z, Cui H, Cai L: **Indocyanine Green-Loaded Polydopamine-Reduced Graphene Oxide Nanocomposites with Amplifying Photoacoustic and Photothermal Effects for Cancer Theranostics**. Theranostics 2016, **6**:1043–1052.
40. Li M, Long S, Kang Y, Guo L, Wang J, Fan J, Du J, Peng X: **De Novo Design of Phototheranostic Sensitizers Based on Structure-Inherent Targeting for Enhanced Cancer Ablation**. J Am Chem Soc 2018, **140**:15820–15826.
41. Hirschhorn T, Stockwell BR: **The development of the concept of ferroptosis**. Free Radic Biol Med 2019, **133**:130–143.
42. Bogdan AR, Miyazawa M, Hashimoto K, Tsuji Y: **Regulators of Iron Homeostasis: New Players in Metabolism, Cell Death, and Disease**. Trends Biochem Sci 2016, **41**:274–286.
43. Hassannia B, Vandenabeele P, Vanden Berghe T: **Targeting Ferroptosis to Iron Out Cancer**. Cancer Cell 2019, **35**:830–849.
44. Song X, Wang X, Liu Z, Yu Z: **Role of GPX4-Mediated Ferroptosis in the Sensitivity of Triple Negative Breast Cancer Cells to Gefitinib**. Front Oncol 2020, **10**:597434.
45. Fucikova J, Kepp O, Kasikova L, Petroni G, Yamazaki T, Liu P, Zhao L, Spisek R, Kroemer G, Galluzzi L: **Detection of immunogenic cell death and its relevance for cancer therapy**. Cell Death Dis 2020, **11**:1013.

46. Yang Y, Tang J, Abbaraju PL, Jambhrunkar M, Song H, Zhang M, Lei C, Fu J, Gu Z, Liu Y, Yu C: **Hybrid Nanoreactors: Enabling an Off-the-Shelf Strategy for Concurrently Enhanced Chemo-immunotherapy**. Angew Chem Int Ed Engl 2018, **57**:11764–11769.
47. Li W, Yang J, Luo L, Jiang M, Qin B, Yin H, Zhu C, Yuan X, Zhang J, Luo Z, et al: **Targeting photodynamic and photothermal therapy to the endoplasmic reticulum enhances immunogenic cancer cell death**. Nat Commun 2019, **10**:3349.
48. Noh I, Son Y, Jung W, Kim M, Kim D, Shin H, Kim YC, Jon S: **Targeting the tumor microenvironment with amphiphilic near-infrared cyanine nanoparticles for potentiated photothermal immunotherapy**. Biomaterials 2021, **275**:120926.
49. Galluzzi L, Vitale I, Warren S, Adjemian S, Agostinis P, Martinez AB, Chan TA, Coukos G, Demaria S, Deutsch E, et al: **Consensus guidelines for the definition, detection and interpretation of immunogenic cell death**. J Immunother Cancer 2020, **8**.
50. Garg AD, Krysko DV, Verfaillie T, Kaczmarek A, Ferreira GB, Marysael T, Rubio N, Firczuk M, Mathieu C, Roebroek AJ, et al: **A novel pathway combining calreticulin exposure and ATP secretion in immunogenic cancer cell death**. EMBO J 2012, **31**:1062–1079.
51. Scaffidi P, Misteli T, Bianchi ME: **Release of chromatin protein HMGB1 by necrotic cells triggers inflammation**. Nature 2002, **418**:191–195.
52. Xue J, Ge H, Lin Z, Wang H, Lin W, Liu Y, Wu G, Xia J, Zhao Q: **The role of dendritic cells regulated by HMGB1/TLR4 signalling pathway in myocardial ischaemia reperfusion injury**. J Cell Mol Med 2019, **23**:2849–2862.
53. Xu J, Xu L, Wang C, Yang R, Zhuang Q, Han X, Dong Z, Zhu W, Peng R, Liu Z: **Near-Infrared-Triggered Photodynamic Therapy with Multitasking Upconversion Nanoparticles in Combination with Checkpoint Blockade for Immunotherapy of Colorectal Cancer**. ACS Nano 2017, **11**:4463–4474.
54. Wang C, Xu L, Liang C, Xiang J, Peng R, Liu Z: **Immunological responses triggered by photothermal therapy with carbon nanotubes in combination with anti-CTLA-4 therapy to inhibit cancer metastasis**. Adv Mater 2014, **26**:8154–8162.
55. Chen W, Guo Z, Zhu Y, Qiao N, Zhang Z, Sun X: **Combination of Bacterial-Photothermal Therapy with an Anti-PD-1 Peptide Depot for Enhanced Immunity against Advanced Cancer**. Advanced Functional Materials 2019, **30**.
56. Kammertoens T, Friese C, Arina A, Idel C, Briesemeister D, Rothe M, Ivanov A, Szymborska A, Patone G, Kunz S, et al: **Tumour ischaemia by interferon-γ resembles physiological blood vessel regression**. Nature 2017, **545**:98–102.
57. Sun W, Wu Y, Zheng M, Yang Y, Liu Y, Wu C, Zhou Y, Zhang Y, Chen L, Li H: **Discovery of an Orally Active Small-Molecule Tumor Necrosis Factor-alpha Inhibitor**. J Med Chem 2020, **63**:8146–8156.
58. Adkins I, Fucikova J, Garg AD, Agostinis P, Spisek R: **Physical modalities inducing immunogenic tumor cell death for cancer immunotherapy**. Oncoimmunology 2014, **3**:e968434.
59. Leone DA, Rees AJ, Kain R: **Dendritic cells and routing cargo into exosomes**. Immunol Cell Biol 2018.

60. Xiang J, Xu L, Gong H, Zhu W, Wang C, Xu J, Feng L, Cheng L, Peng R, Liu Z: **Antigen-Loaded Upconversion Nanoparticles for Dendritic Cell Stimulation, Tracking, and Vaccination in Dendritic Cell-Based Immunotherapy**. ACS Nano 2015, **9**:6401–6411.
61. Lian H, Guan P, Tan H, Zhang X, Meng Z: **Near-infrared light triggered multi-hit therapeutic nanosystem for tumor specific photothermal effect amplified signal pathway regulation and ferroptosis**. Bioactive Materials 2021.
62. Zhou F, Feng B, Yu H, Wang D, Wang T, Ma Y, Wang S, Li Y: **Tumor Microenvironment-Activatable Prodrug Vesicles for Nanoenabled Cancer Chemoimmunotherapy Combining Immunogenic Cell Death Induction and CD47 Blockade**. Adv Mater 2019, **31**:e1805888.

Scheme

Scheme 1 is available in supplementary section.

Figures

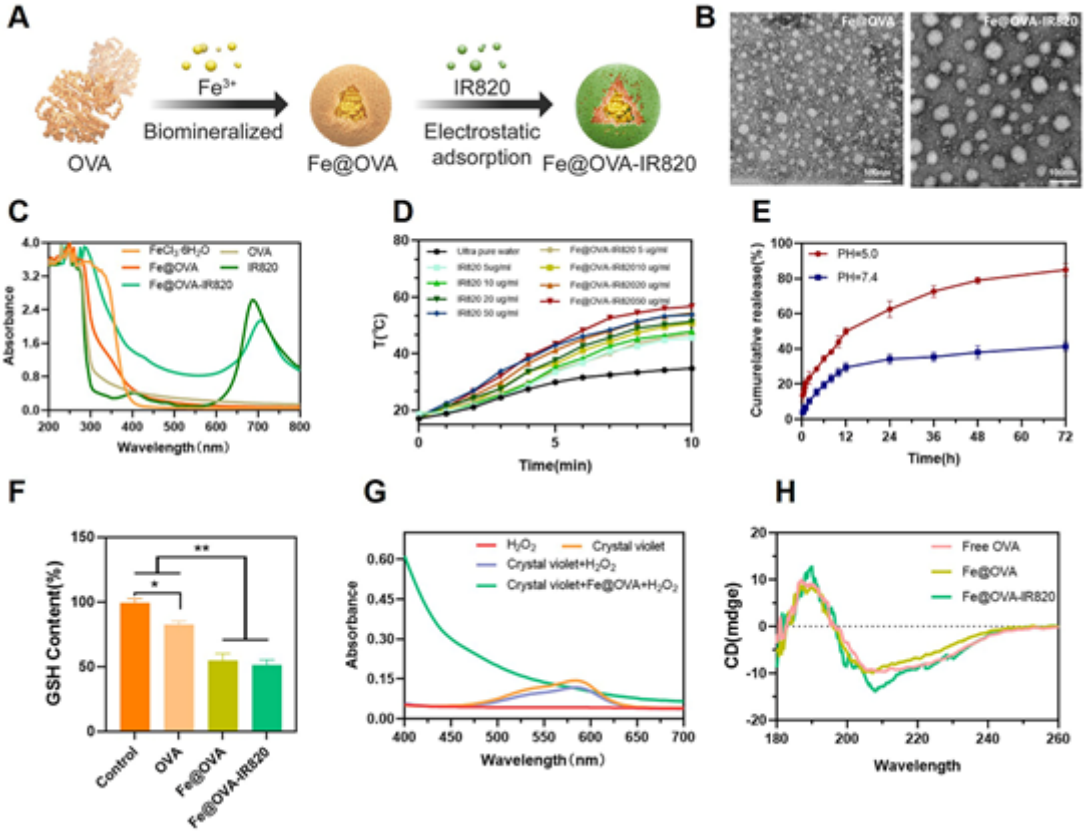

Figure 1

(A) Preparation process of Fe@OVA-IR820 nanovaccine. (B) The TEM image after phosphotungstic acid staining of Fe@OVA and Fe@OVA-IR820 nanoparticles. Bar, 100 nm. (C) Ultraviolet absorption spectrum of each material during the preparation process. (D) The photothermal performance of water, free IR820

and Fe@OVA-IR820 nanoparticles under different IR820 concentrations with irradiation power of 2.5 W/cm^2. (E) Cumulative release curve of iron ions from nanovaccines with different pH values. (F) Consumption of GSH by different nanoparticle groups in vitro experiments. (G) Effect on the characteristic absorption peak of crystal violet of different nanoparticle preparation groups. (H) Circular dichroism of free OVA, Fe@OVA and Fe@OVA-IR820 nanoparticles.

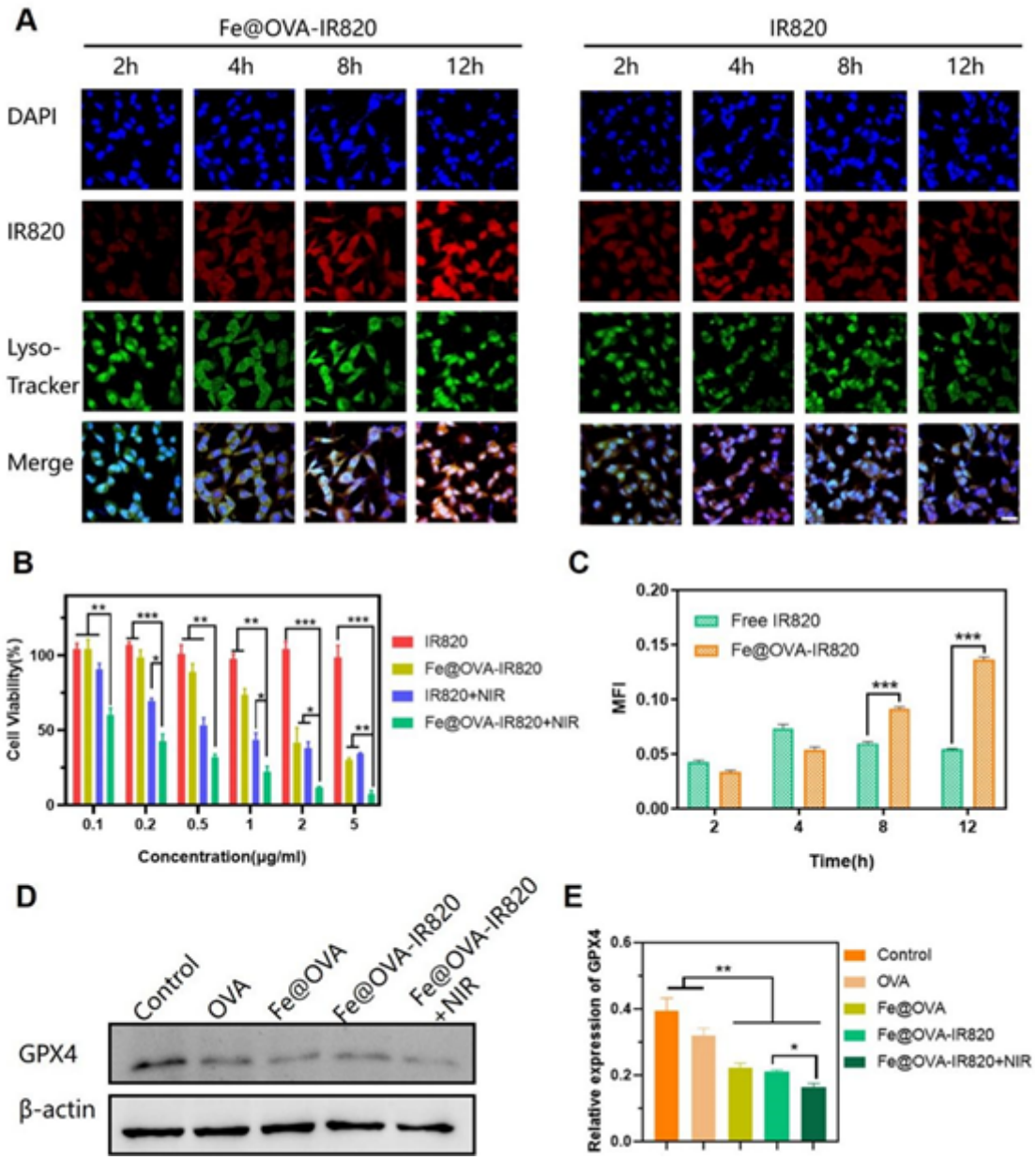

Figure 2

(A) Time-dependent cellular uptake image of free IR820 and Fe@OVA-IR820 in B16-OVA cells. Scale, 50 μm. (B) Relative viabilities after incubated with free IR820 and Fe@OVA-IR820 at different concentrations and irradiated for 5 minutes. (C) Fluorescence semi-quantitative analysis of IR820 signal in A (n = 3). (D) Expression of glutathione peroxidase 4 protein in B16-OVA cells detected by western blot after incubated

in different preparation groups for 24 hours. (E) Semi-quantitative analysis of gray-scale images of GPX4 protein bands.

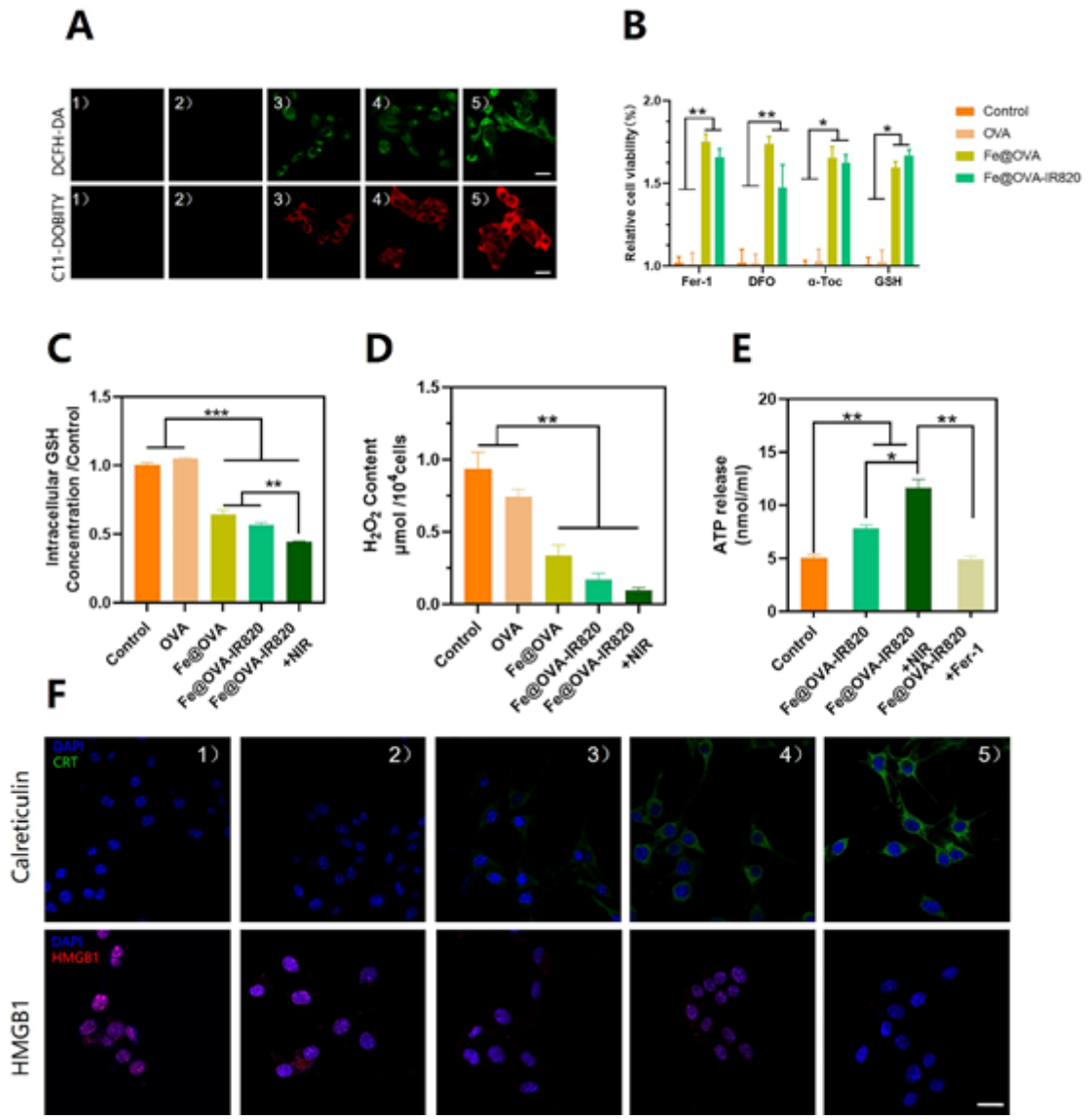

Figure 3

(A) Levels of ROS and LPO in B16-OVA cells were detected respectively via LSCM. Scale, 25 μm. (B) Relative cell viability of B16-OVA cells with ferroptosis pathway related inhibitors, which were validated by adding ferrostatin-1, deferoxamine, α-tocopherol and glutathione. The data is shown as mean ± SD (n = 3). The levels of GSH(C), H_2O_2(D), and ATP (E) released in B16-OVA cells after treated with different preparation groups for 24 hours. (F) Immunofluorescence signal acquisition of calreticulin (above) and HMGB1 (below). Scale, 50 μm.

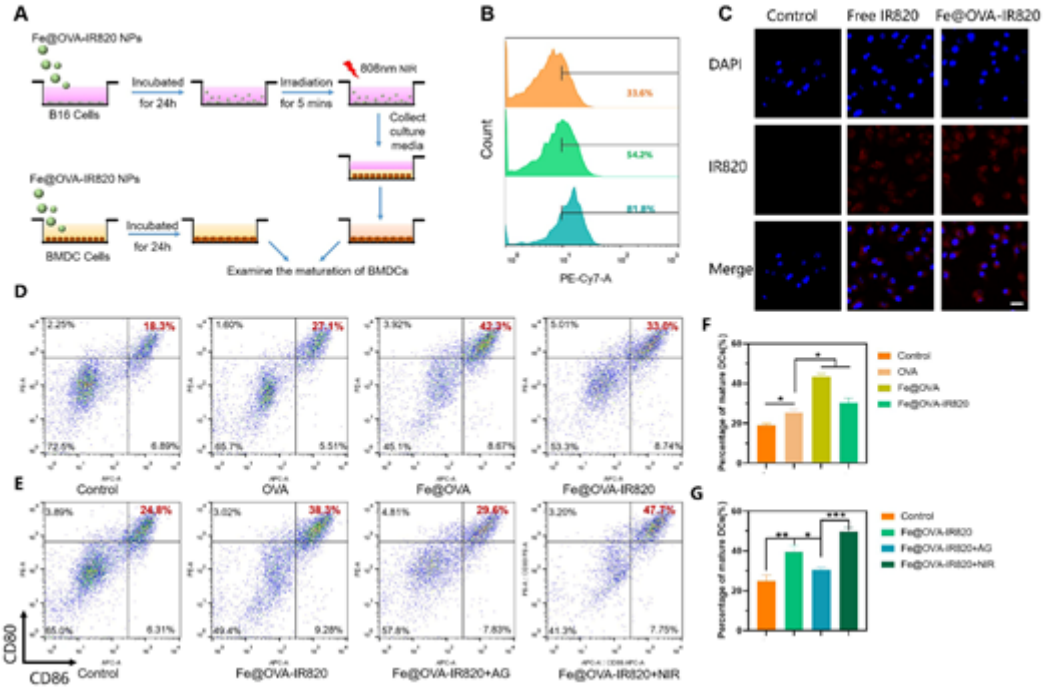

Figure 4

(A) Schematic diagram of the maturation of nanovaccine-treated B16-OVA tumor cell lysates and bone marrow derived cells (BMDCS) directly stimulated by nanovaccine. CD11c-positive dendritic cells were gated by flow cytometry. Scale, 50 μm. Flow cytometry picture (B), confocal microscopy image(c) of nano vaccine uptake by dendritic cells. The results of promoting the maturation of dendritic cells treated with different formula groups (D) and the addition of B16-OVA cell culture medium treated with different formula groups (E) were demonstrated. Percentage of mature DC cells incubated directly (F) and indirectly (G) with different formulations for 24 h.

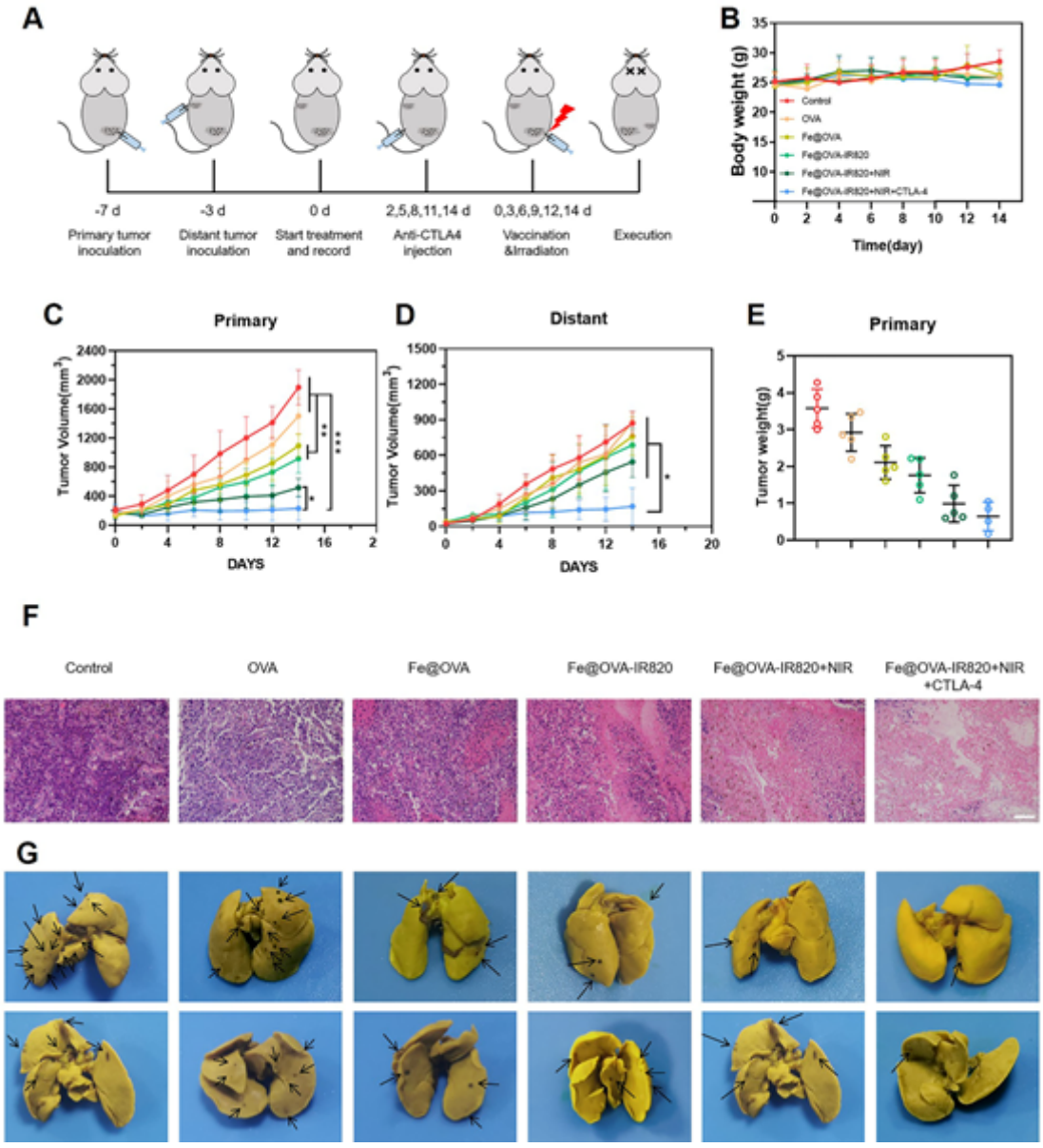

Figure 5

(A) Schematic of distant tumor growth inhibited by nanovaccine combination therapy. Changes in C57BL/6 mice body weight (B), primary tumor volume (C) and distal tumor volume (D) were observed every twice day. The weight of primary tumor (E) and H&E staining results (F) were recorded after the autopsy. Scale, 100 μm. (G) Representative photographs of lung metastasis in B16-OVA tumor model.

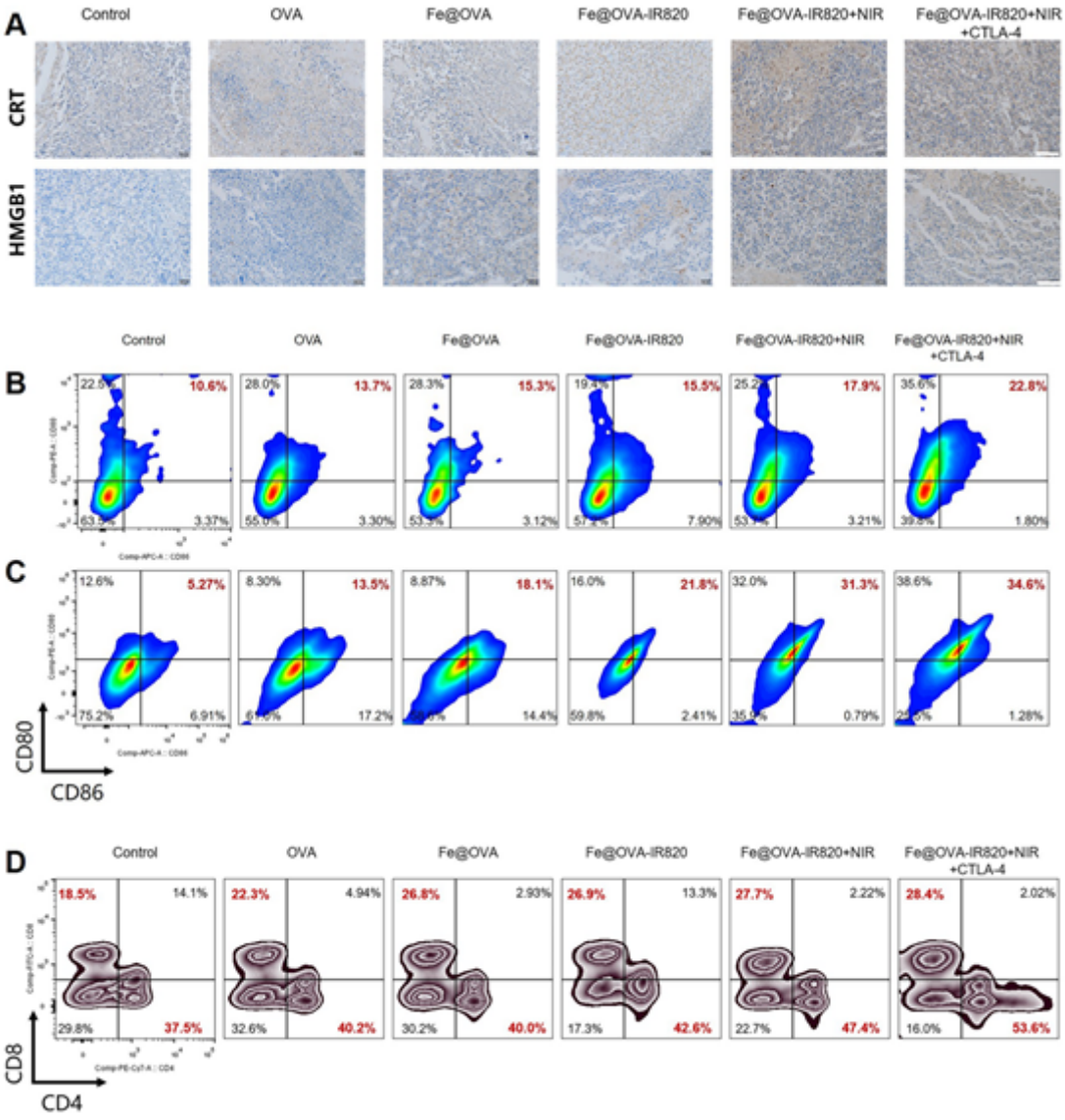

Figure 6

(A) Representative image of B16-OVA after biopsy of the primary tumor, showing increased release of ICD markers. Scale: 50 μm. Representative graphs of DC maturation of C57BL/6 mice in draining lymph nodes (B) and tumors (C). (D) Detection of Splenic T cells (CD3+/CD4+ or CD3+/CD8+) in C57BL/6 mice with B16-OVA tumor.

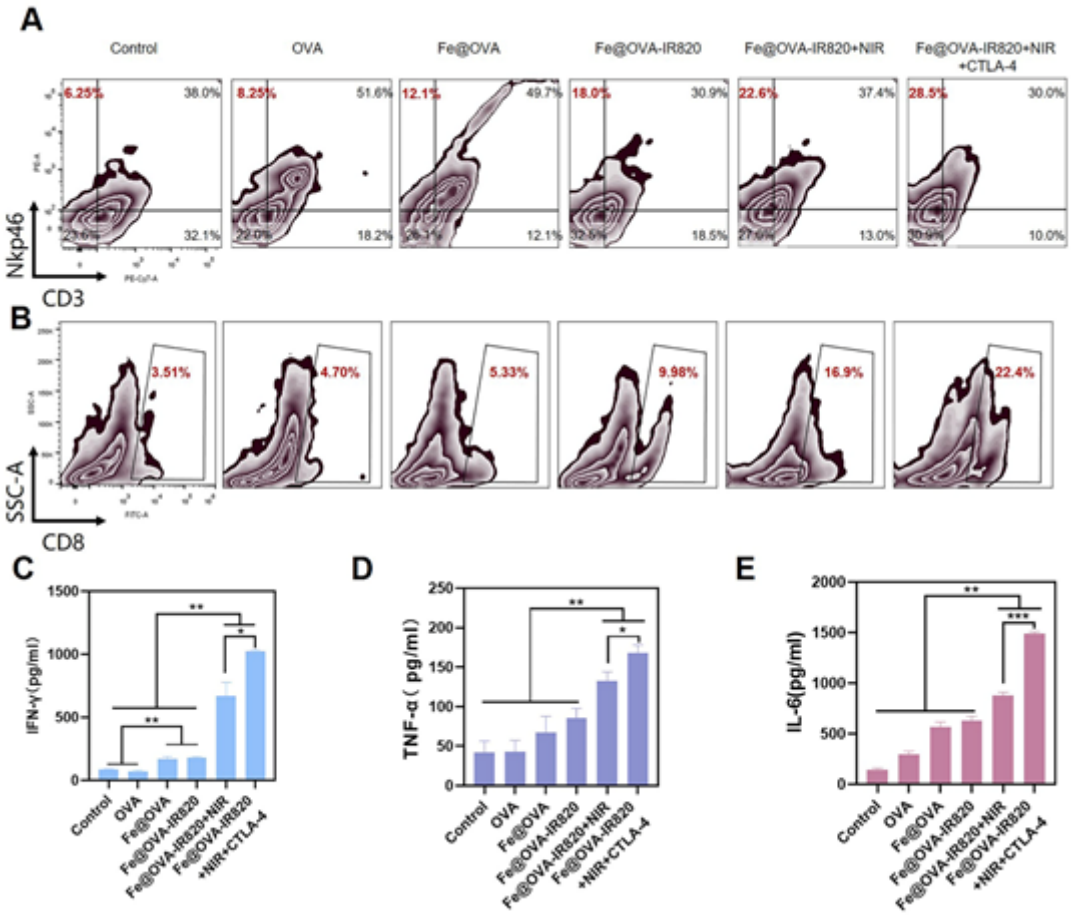

Figure 7

Infiltration of NK cells (A) andCD8+ T lymphocytes (B) in tumor site in different drug administration groups were determined after execution. ELISA analysis of IFN-γ(C), TNF-α(D) and IL-6 (E) levels in primary tumors of C57BL/6 mice (n = 3).

Supplementary Files

This is a list of supplementary files associated with this preprint. Click to download.

- SupportingInformation.doc
- floatimage1.jpeg